Protonation Effects on the Equilibrium and Dynamical Properties of the Alanine Tetrapeptide

Herb D. Blatt,[†] Paul E. Smith,[‡] and B. Montgomery Pettitt*,[†]

Chemistry Department, University of Houston, Houston, Texas 77204-5641, and Department of Biochemistry, Kansas State University, Manhattan, Kansas 66506-3702

Received: April 17, 1997[⊗]

The effect of terminal group charge on the structure and dynamics of the alanine tetrapeptide has been investigated using molecular dynamics simulations. Neutral and positive N-termini, together with neutral and negative C-termini, were studied, resulting in a total of four 10 ns simulations with different terminal group charge combinations. Analysis of these simulations indicates that the terminal group charge has only a minor effect on the conformations sampled for the central dihedrals, but a significant effect on the population distribution of the dihedrals close to the terminal groups. The conformational distribution at the C-terminus (ψ_3) was also found to depend on the charge at the N-terminus. Here, the differences result from the formation of transient ion pairs (salt bridges) in the zwitterion case. However, equilibrium sampling of these intramolecular ion pairs was still not fully converged even after 10 ns.

Introduction

It is widely thought that the conformations available to a peptide in solution determine many characteristics of binding to a receptor/inhibitor site.[1] For this reason, many methods (X-ray diffraction, NMR, etc.) are utilized in an attempt to elucidate the important (highly populated) conformations of peptides in solution.[2] Many simple nonpolar peptides are often insoluble, or only sparingly soluble, in water or salt solution. Hence, to increase the solubility of peptides, it is typical to vary either the buffering solution composition or the pH or to chemically modify the peptide using various terminal groups. In so doing it is often assumed that these variations/modifications do not significantly affect the conformational preferences of the peptide. However, there are many experimental results that indicate that the charge state of both side chains[3] and terminal groups[4] can dramatically alter the conformational preferences of oligopeptides. Dyson *et al*.[5] reported that interaction between end groups has an effect on the turn populations of a peptide in solution. The results from an *ab initio*[6] theoretical study of alanine peptides in the gas phase indicate that interaction between the terminal groups can significantly affect the torsional states of other residues.

Here we investigate the conformational distribution of a small model peptide in solution as a function of the charge state of each terminus, *i.e*. pH, at the microscopic level using molecular dynamics simulations. A model peptide (the alanine tetrapeptide) in explicit solvent was used for the studies. The alanine tetrapeptide was chosen due to its structural simplicity, while retaining important features common to all amino acids, and to compare with other theoretical studies of alanine chains of varying lengths.[7−14] Both thermodynamic (equilibrium populations) and kinetic (transition rate) properties have been examined. In the following section we present the simulation details and compounds and models used. The results of four 10 ns simulations in explicit solvent are then presented and subsequently discussed in relation to previous work and each other. Our conclusions follow.

Method

Four molecular dynamics simulations of the alanine tetrapeptide were performed with the following end group combinations: $NH_3^+-ALA_4-CO_2H$ (+/0), $NH_2-ALA_4-CO_2H$ (0/0), $NH_2-ALA_4-CO_2^-$ (0/−), $NH_3^+-ALA_4-CO_2^-$ (+/−). We will refer to the peptide using the simplified notation denoted in parentheses. The explicit aqueous solvent model TIP3P[15] was used in a cubic box of 25 Å length using periodic boundary conditions. The CHARMM24 all-atom force field[16] was used for all simulations. The electrostatic interactions were calculated using an Ewald sum[17] ($\alpha = 0.25$ Å^{-1}, $R_c = 12$ Å, $n^2_{max} = 49$). The Ewald sum was chosen as the method for calculating the electrostatic interactions since it has been shown to significantly reduce artifacts associated with the use of cutoffs and switching functions.[18,19] SHAKE[20] was used to constrain all bond lengths. The simulations were prepared by pre-equilibrating a box of 512 TIP3P water and placing the solute with the greatest number of atoms (+/0) into the center of the box, which contained 496 water molecules after removing the waters in close contact (≤2.3 Å) with the peptide. The subsequent simulations were prepared by removing the appropriate atoms and changing the charges of the peptide to obtain the desired end group combinations. Each of the simulations were then minimized with 10 steps of steepest descent and equilibrated independently using the following procedure; 5 ps with solute held still, reassigning solvent velocities every 0.25 ps, followed by 35 ps with solute held still, reassigning solvent velocities every 2.5 ps, and then 10 ps with solvent held still, reassigning solute velocities every 0.5 ps. The initial configuration of each of the peptides in all four simulations was fully extended (all trans) and each simulation ran for 10 ns in the microcanonical (NVE) ensemble using a 2 fs time step. Analysis was performed on data collected every 0.1 ps.

Potentials of mean force (PMF) for rotation around the dihedral degrees of freedom were generated using the following procedure for each simulation. The ϕ/ψ density map was coverted to a 2D probability map with a grid separation of 20°, giving a total of 18^2 grid points. The highest probability grid point was used to determine the zero of the PMF, which is then subtracted from the PMF calculated at each point

[†] University of Houston.
[‡] Kansas State University.
[⊗] Abstract published in *Advance ACS Abstracts,* July 15, 1997.

S1089-5647(97)01333-3 CCC: $14.00

TABLE 1: Averages and Fluctuations[a]

	+/0	0/0	0/−	+/−
E_{uu} (kJ/mol)	434 ± 20	483 ± 18	520 ± 19	41 ± 65
E_{uv} (kJ/mol)	−528 ± 36	−388 ± 31	−720 ± 43	−791 ± 123
E_{vv} (kJ/mol)	−20 215 ± 103	−20 374 ± 128	−20 185 ± 114	−20 021 ± 140
E_k (kJ/mol)	61 ± 7	57 ± 7	58 ± 7	62 ± 7
T (K)	294 ± 7	291 ± 7	293 ± 7	298 ± 7
P (atm)	−213 ± 550	−260 ± 548	−302 ± 552	−216 ± 556
D_v (m^2/s) × 10^{-9}	4.9 ± 0.1	4.4 ± 0.1	4.5 ± 0.1	4.9 ± 0.1
N_1 to C_4 (Å)	9 ± 2	9 ± 2	9 ± 2	8 ± 3

[a] E_{uu} solute−solute potential energy; E_{uv} solute−solvent potential energy; E_{vv} solvent−solvent potential energy; E_k k-space energy; D_v solvent diffusion coefficient; average N_1 to C_4 tetrapeptide end-to-end distance.

along the ψ rotation.

$$\Delta W = -k_b T \ln[p(\phi_i,\psi_i)] + k_b T \ln[p^*(\phi,\psi)]$$

where $p^*(\phi,\psi)$ is the most probable state, k_b = Boltzmann constant, T = 300 K, and ΔW was calculated along $\phi = -80°$ (see Results and Discussion section).

Kinetic analysis of dihedral angle rotation was performed using the correlation function approach outlined by Zhang and Pastor.[21]

Results and Discussion

In this section the outcomes of the four simulations are presented and compared with each other. Energetics, dynamics, and structure are considered in detail.

A. Energetics and Dynamics. Table 1 lists the energetic and structural averages, together with their rms fluctuations, obtained from each of the four 10 ns simulations. The solute intramolecular potential energy is similar for the neutral and single-charged end group simulations, but is noticeably lower for the zwitterion. The solute−solvent interaction appears to be more stabilizing for the negatively charged C-terminus simulations. Energy fluctuations are also noticeably larger for the zwitterionic system.

The solvent self-diffusion coefficients were similar for all the systems and roughly follow the trend in the average temperatures. The diffusion coefficients are in the range (4.4−4.9) × 10^{-9} m^2/s. These values are larger than that observed for experimentally determined values for pure water,[22,23] ≈2.5 × 10^{-9} m^2/s. The self-diffusion of water for a system containing a biological solute is expected to be slower than that of pure water.[23] However, other MD studies using the TIP3P water model have reported similar values.[18,24] This does not appear to be strongly related to the use of the Ewald sum since Tasaki *et al.*[24] observe values of (4.15−4.59) × 10^{-9} m^2/s using switching and shifting functions for the truncation of long-range interactions. However, certain truncation schemes do create potential artifacts affecting dynamics and diffusion[25] especially for highly charged groups.

B. Liquid Structure. Distribution functions have been calculated for the solvent around each group in each charge state. The radial distribution functions (rdf's) displayed in Figure 1 show that the charged end group simulations display a higher relative probability of observing water in the first two solvation shells (see the first two peaks), but after ≈7 Å the solvent distribution becomes independent of the charge. As expected, the distance from the terminal groups to the first minima and maxima occur at shorter distances for the charged end groups (see Table 2), indicating a more favorable interaction with the solvent. The coordination numbers calculated from the rdf's are also reported in Table 2. The average number of waters coordinated to the N-terminus in the zwitterion is slightly less than that compared to the (+/0) simulation, and the same

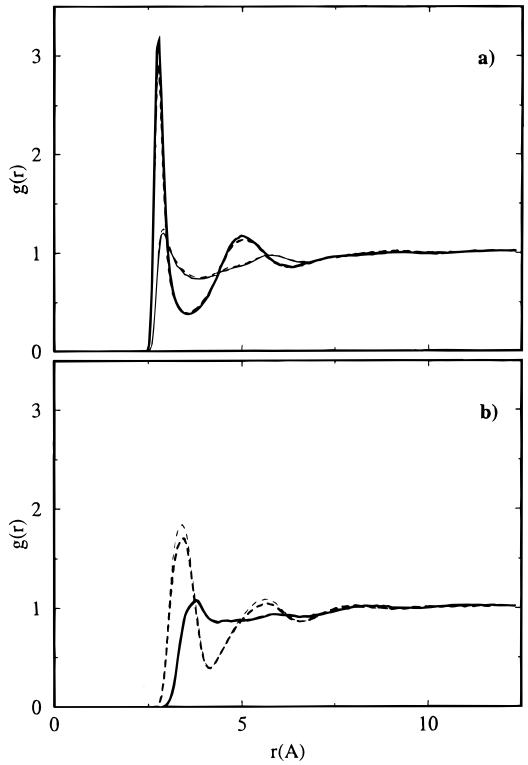

Figure 1. Radial distribution functions (a) N_1 to water oxygen, (b) C_4 to water oxygen: (+/0) thick solid line, (0/0) thin solid line, (0/−) thin dashed line, (+/−) thick dashed line.

TABLE 2: Radial Distribution Functions[a]

r (Å)	+/0	0/0	0/−	+/−
g_{NO}^{max}	2.8	2.9	2.9	2.8
g_{NO}^{min}	3.6	3.8	3.8	3.5
n_{NO}^{min}	4.4	4.5	4.6	4.0
g_{CO}^{max}	3.8	3.8	3.4	3.4
g_{CO}^{min}	4.3	4.4	4.2	4.2
n_{CO}^{min}	6.1	6.5	7.3	6.8

[a] g_{NO} is the rdf for N-terminus to water oxygen, g_{CO} is the rdf for C-terminus to water oxygen; n_{NO}^{min} is coordination number for nitrogen atom of N-terminus integrated to g_{NO}^{min}; n_{CO}^{min} is coordination number for carbon atom of C-terminus integrated to g_{CO}^{min}, where min and max are the first minima and maxima, respectively, of the rdf.

is true for the C-terminus of the zwitterion compared to the (0/−) simulation. This is due to the fact that the zwitterion can form a transient salt bridge between the two charged end groups (see the Structure section), which decreases the average number of water molecules that can coordinate to each end of the peptide. The coordination numbers for the N^+ terminal groups are comparable to previous values of Smith *et al.*[26] which were calculated from an MD simulation of the bis(penicillamine) enkephalin zwitterion in explicit solvent. In that study, with a

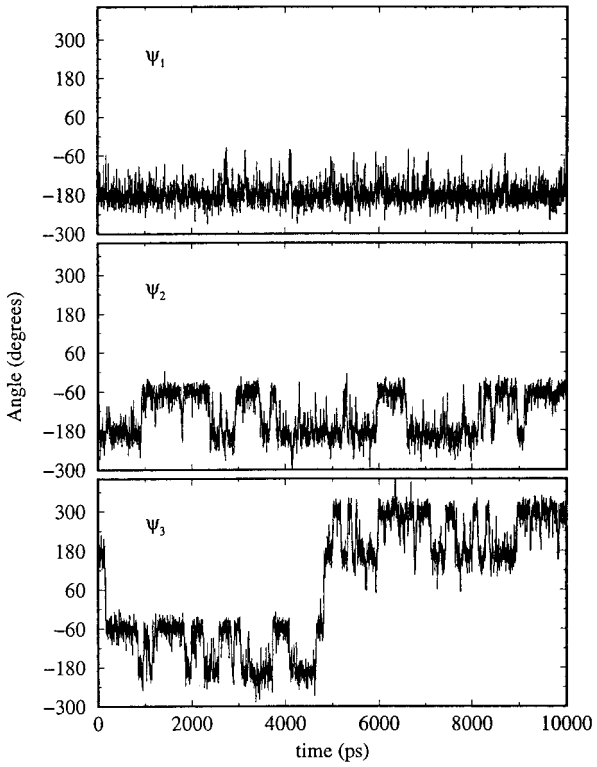

Figure 2. Time history of ψ dihedrals from the (+/−) simulation.

different potential surface the authors report a value for the N^+ to water oxygen coordination number of 3.8, while our values were 4.0 and 4.4 for the (+/−) and (+/0) simulations, respectively. Thus the difference in the opposite end charge state has a significantly larger effect than the change in potential surface.

C. Conformational Sampling. The conformations sampled by the peptides in each of the four simulations were limited to transitions of the three ψ dihedrals, as expected from the time scale for ϕ transitions for the alanine dipeptide.[27] Figure 2 shows the time history of the backbone ψ dihedrals for the (+/−) simulation and is representative of the behavior of these dihedrals in all four simulations. Conformational sampling of the ϕ dihedrals remained around −80° throughout the simulations. Results from the study by Smith *et al.*[27] of the alanine dipeptide show that the time scale for ϕ dihedral transitions was on the order of 10 ns. We therefore obtained a complete subset of the possible conformations of the tetrapeptide for this time scale. The two central residue ψ dihedrals, ψ_2 and ψ_3, each have transitions between two populations at −60° and 165°, respectively. All four simulations showed similar transitions for ψ_2 and ψ_3.

The ψ/ϕ density maps of the two central residues from the (+/−) simulation (Figure 3) display the distributions resulting from the conformational sampling for all dihedrals, which was qualitatively similar for all the simulations. Two populations for each of the central ψ dihedrals are apparent in this plot. As previously mentioned, the sampling around ϕ was restricted. We therefore defined four major conformational states to describe the highly populated conformations of the peptides in our simulations corresponding to different backbone combinations in the two populated regions of the Ramachandran diagram (α_R and β). Figure 3c,d shows these combinations of ψ_2 and ψ_3 and their designations as states 1 through 4 with state 1 ≡ $\phi_2/\psi_2 \approx -80°/-60°$ and $\phi_3/\psi_3 \approx -80°/-60°$; state 2 ≡ $\phi_2/\psi_2 \approx -80°/-60°$ and $\phi_3/\psi_3 \approx -80°/165°$; state 3 ≡ $\phi_2/\psi_2 \approx -80°/165°$ and $\phi_3/\psi_3 \approx -80°/-60°$; state 4 ≡ $\phi_2/\psi_2 \approx -80°/165°$ and $\phi_3/\psi_3 \approx -80°/165°$.

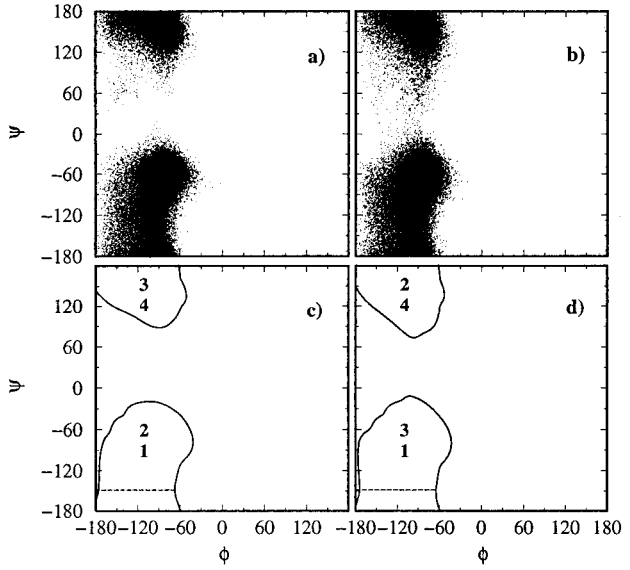

Figure 3. ϕ,ψ density maps for the two central residues from the (+/−) simulation, (a) ψ_2/ϕ_2, (b) ψ_3/ϕ_3; and state definitions, (c) ψ_2/ϕ_2, (d) ψ_3/ϕ_3.

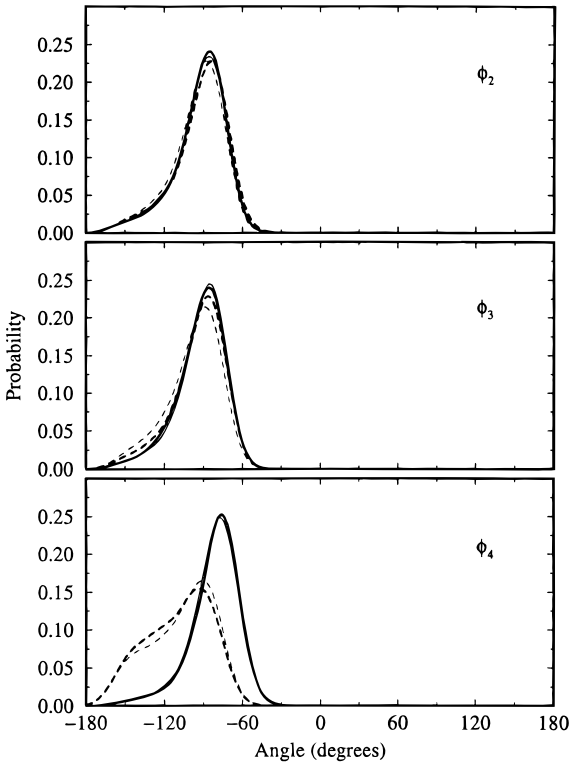

Figure 4. Normalized probability distribution of ϕ dihedrals: (+/0) thick solid line, (0/0) thin solid line, (0/−) thin dashed line, (+/−) thick dashed line.

Figure 4 is a histogram of the three ϕ dihedrals from which can be seen that the probability distributions of ϕ_2 and ϕ_3 are very similar for each of the four simulations. However, the distributions of ϕ_4 for the negatively charged C-terminus simulations (0/−) and (+/−) are less restricted compared to the neutral C-terminus simulations. This indicates greater flexibility of the ϕ dihedral closest to the negatively charged C-terminus.

Sampling around ψ_1 is not the same for all the simulations, as shown in Figure 5. The positively charged N-terminus simulations (+/0) and (+/−) have one populated region centered at 165°, while the neutral N-terminus simulations (0/0) and (0/−) have two populated regions at 165° and −60°. The

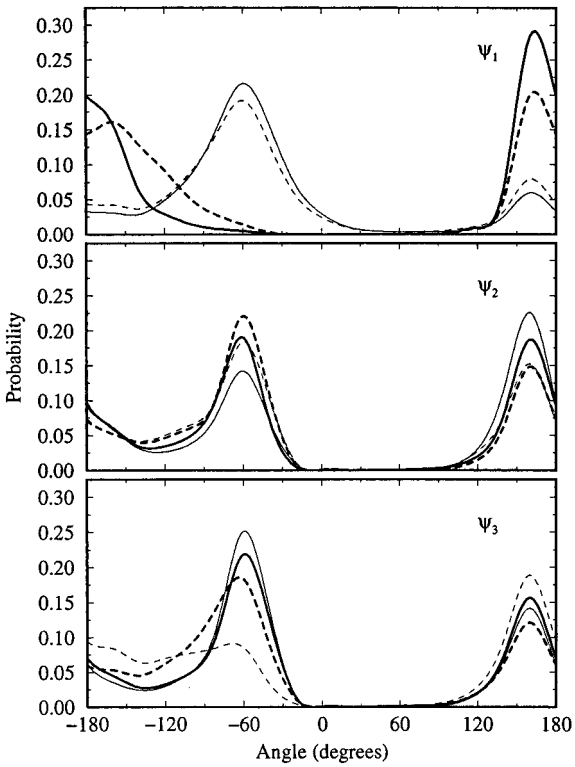

Figure 5. Normalized probability distribution of ψ dihedrals: (+/0) thick solid line, (0/0) thin solid line, (0/−) thin dashed line, (+/−) thick dashed line.

histograms for ψ_2 and ψ_3 show that the highly populated regions of these dihedrals are the same for all four simulations but differ in the degree of population.

An alternative method of visualizing the sampling of the tetrapeptide simulations is through the use of a Θ,Y map.[28] The Θ,Y map is a projection of the conformation of a segment of a peptide or protein that extends over four successive C_α atoms onto a two-dimensional surface. Θ is a pseudodihedral defined by the dihedral formed between four successive C_α atoms along the peptide backbone. This degree of freedom describes the general degree of folding along that segment. The second degree of freedom Y is the triple scalar product of three unit vectors, each of which corresponds to one of the three planar peptide groups (CO−NH) along the four-residue segment. Y ranges in value from −1 to 1 and describes the orientation of these groups in relation to one another. Figure 6 is the Θ,Y map of the (+/−) simulation, which is similar for each of the four simulations. There are two main areas of density in this map, one centered at Θ/Y ≈ 25°/−0.1, indicating turn/folded conformations, and the second region centered at Θ/Y ≈ −120°/+0.2, representing extended structures. The turn/folded region is populated by structures from states 1 and 2, while the extended region is populated by states 3 and 4. In this way we find groupings based on the two dominant shapes of the backbone.

D. Structure. The four states that were populated by each of the simulations ranged from turns with short end-to-end distances to fully extended structures. We did not observe any significant or stable classically defined reverse turn conformations in our simulations. Analysis of each frame of the trajectories by comparison of the ϕ/ψ values to those defined for the different types of reverse turns and allowing a tolerance of ±10° resulted in only less than 2% of the frames classified as a reverse turn. The average end-to-end distance increases from state 1 through state 4. None of the simulations became trapped within a particular state; each has established an equilibrium between the four observed states. Figure 7a displays

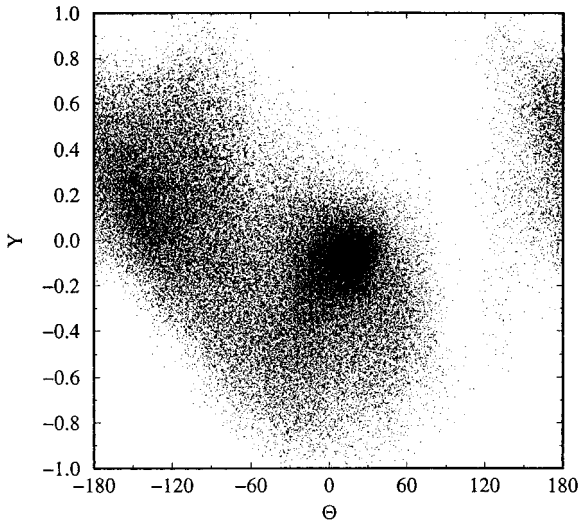

Figure 6. Θ,Y density map of the (+/−) simulation.

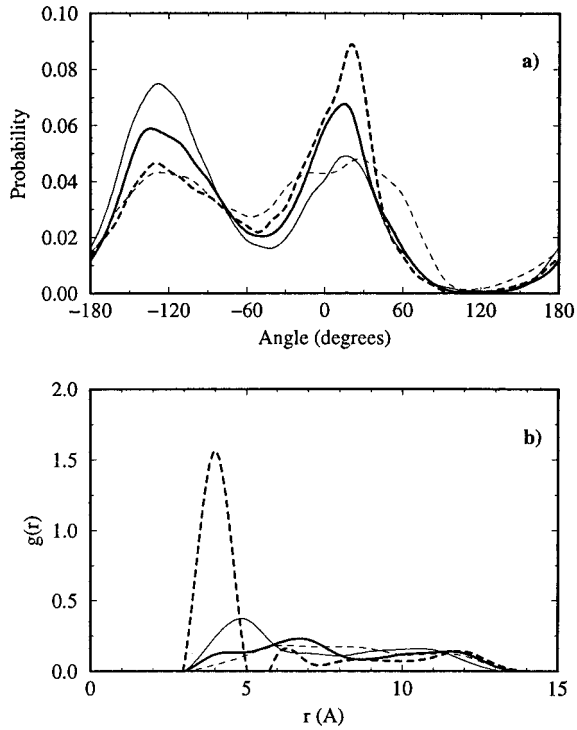

Figure 7. (a) Normalized probability distribution of the C_α dihedral and (b) normalized probability distribution of the end-to-end distance (N to C_4): (+/0) thick solid line, (0/0) thin solid line, (0/−) thin dashed line, (+/−) thick dashed line.

the Θ (normalized C_α pseudodihedral) probability distribution for each simulation and, as previously mentioned, gives a general indication of the degree of folding along a four-residue segment of the peptide backbone. There are two main populated regions centered at ≈25° and ≈−120° representing folded and extended structures, respectively. The zwitterion strongly preferred folded conformations, while the (0/0) simulation preferred extended conformations. The other simulations that had only one charged end group (+/0) and (0/−) do not show a strong preference for folded over extended or vice versa.

Figure 7b is a normalized histogram for the end-to-end distance for each of the simulations. The distributions of end-to-end distances for each of the simulations are similar in range but differ in population. The zwitterion simulation (+/−) had the greatest population of short end-to-end distances compared to the other simulations. This trend is also reflected in the average end-to-end distance reported in Table 1, which is

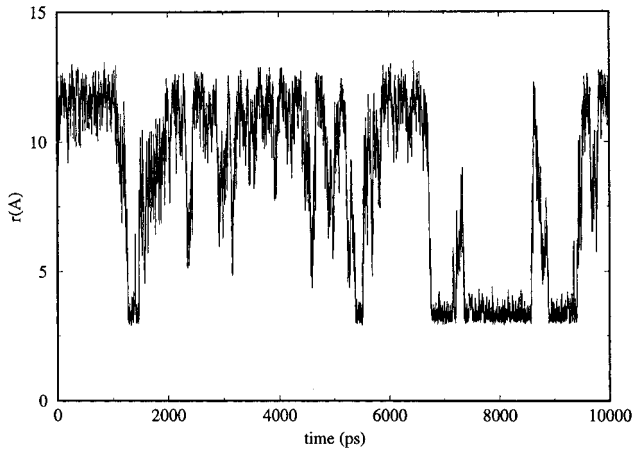

Figure 8. Time history of the end-to-end distance (N_1 to C_4) from the (+/−) simulation.

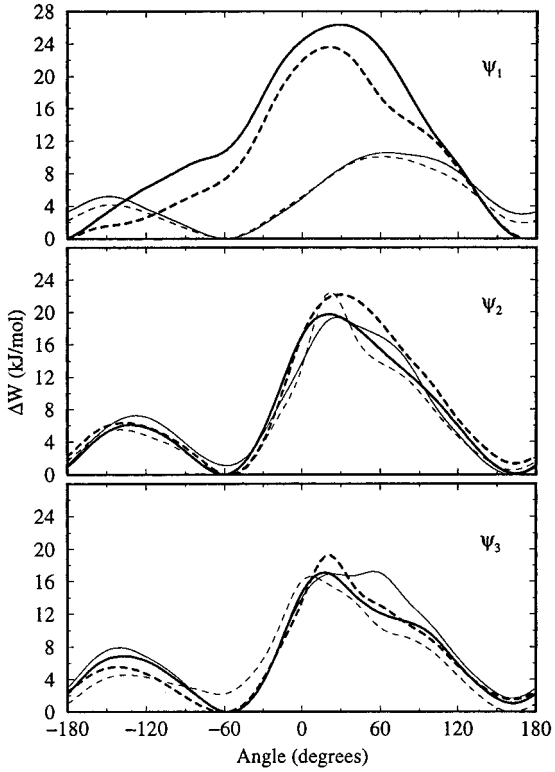

Figure 9. Potential of mean force for the ψ dihedrals: (+/0) thick solid line, (0/0) thin solid line, (0/−) thin dashed line, (+/−) thick dashed line.

slightly shorter for the zwitterion since it can form favorable interactions between the two charged end groups. Although it is energetically favorable for the two charged terminal groups to interact in the zwitterion, there must be associated entropic and desolvation penalties. The time history of the end-to-end distance for the zwitterion (Figure 8) shows that this simulation spent a considerable amount of time in conformations with large distances between the two terminal groups and did not become trapped in a conformation with a salt bridge between the ends of the peptide. The time scale for formation of the tethered ion paired conformations was very long, often exceeding 4 ns. Once formed, these ion pair configurations remained stable for as long as 1−1.5 ns.

E. PMF. Figure 9 displays the calculated potential of mean force for the three ψ dihedrals from each of the simulations, and Table 3 gives the relative values of the minima and maxima. As noted earlier, the positively charged N-terminus simulations displayed only one free energy minima for ψ_1 rotation. The

TABLE 3: Relative Conformational Free Energies (kJ/mol) and ψ Rotational Correlation Times (ps)[a]

	conformation			+/0	0/0	0/−	+/−
ψ_1		−150	max		5.2	4.1	
	g⁻	−60	min		0.0	0.0	
		60	max		10.5	10.0	
	t	165	min		3.0	2.0	
τ			t→g⁻		6	6	
			g⁻→t		40	32	
ψ_2		−135	max	6.1	7.1	5.5	6.3
	g⁻	−60	min	0.0	1.1	0.0	0.0
		30	max	19.3	19.2	20.8	22.2
	t	165	min	0.1	0.0	0.5	1.3
τ			t→g⁻	83	72	60	62
			g⁻→t	69	61	52	94
ψ_3		−135	max	6.9	7.8	4.6	5.5
	g⁻	−60	min	0.0	0.0	2.3	0.0
		30	max	16.0	16.8	14.7	17.9
	t	165	min	1.0	1.7	0.0	1.5
τ			t→g⁻	68	61	50	47
			g⁻→t	56	67	23	34

[a] Error in minima > 1 kJ/mol, error in maxima 2−3 kJ/mol. Correlation time error ≈ ±5 ps. τ = rotational correlation time given by $[c] = [c]_0 e^{-t/\tau} \equiv e^{-kt}$, where $[c]$ is concentration of the trans isomer, t is time, and k is the rate constant for the dihedral transition (see Zhang and Pastor[21]).

PMFs for ψ_2 and ψ_3 have two minima (−60° and 165°), α_R and β, respectively. The two barriers separating the minima are at 30° and −135°; however the majority of the transitions occur over the latter. Comparison of the minima and maxima of the PMF for the rotation around ψ_2 between the four simulations does not show any correlation with end group charge combination. The same comparison for ψ_3 indicates a correlation between the C-terminal charge state and the height of the barrier at $\psi = -135$. The relative PMF values at this barrier are lower for the negatively charged C-terminus simulations.

The correlation times for the ψ dihedral transitions were calculated and tabulated in Table 3. Here, the minima ≈−60° corresponds to gauche⁻ (g⁻) and at 165° to trans (t) conformations. Although the barrier height at $\psi \approx 30°$ is listed for ψ_2 and ψ_3, as previously mentioned, the majority of the transitions between the two minima occur over the barrier at $\psi \approx -135°$. The ψ_1 correlation times are reported only for the neutral N-terminus simulations (0/0) and (0/−) since the other simulations possess only one minimum for ψ_1. ψ_2 does not show a correlation between the end group charge type and the rotational correlation time τ. ψ_3 shows a correlation between τ and the C-terminus charge type; the negatively charged C-terminus simulations (0/−) and (+/−) have a faster rotational correlation time than the neutral C-terminus simulations. Therefore the correlation between τ and end group charge follows the same trend as the PMF analysis.

In the study of helix propagation by Young and Brooks[7] umbrella sampling was performed on Ace−$(Ala)_n$−NMe (n = 4, 5, 10, 15) and free energy surfaces calculated for rotation about the N- and C-terminal ψ dihedrals. The free energy surfaces from that study have minima at −45° and 136° and two barriers at −120° and 30°. The authors attribute the barrier at −120°, which in our study is slightly shifted to −135°, to unfavorable steric and electrostatic interactions between the carbonyl oxygen atoms on the first and second residues and unfavorable steric interactions between the β carbon on the second residue and the amide hydrogen on the third residue. Those authors also attribute the barrier at 30° to unfavorable steric interactions between the amide hydrogen on the first residue and the carbonyl oxygen on the third residue. In our

PMFs the barrier at 30° is the higher barrier, in contrast to that of Young *et al*.,[7] where it is the lower of the two barriers. The minima of the PMFs in our study are in the same general region as Young *et al*.[7] but slightly shifted. The majority of the differences in the PMFs for the ψ dihedrals between these two studies are almost certainly due to the differences in the parameter sets used for the peptides. We used the CHARMM24 all-atom parameters, while Young and Brooks used the CHARMM19 extended atom parameter set.

Tobias and Brooks[8] studied the conformational equilibrium of the alanine "dipeptide" in the gas phase and in aqueous solution using MD with the CHARMM19 parameter set and TIP3P water model. Comparison of our PMF for the alanine tetrapeptide to the free energy profile between the α_R and the β conformations of Tobias and Brooks shows that the minimum energy path along $\phi = -80°$ agrees with our study. The general placement of minima along rotation in the ψ dihedral are in general agreement with our study, but the transitions occur over the equivalent to the higher energy barrier in our study, as is consistent with our observation about the difference in potential surface.

We compared the Ramachandran plots from our simulations (Figure 3) to those of other MD studies of polyalanine peptides: alanine "dipeptide", Anderson and Hermans,[9] Marrone *et al*.;[10] Ac−$(Ala)_2$−NHMe, Tobias *et al*.; Ac−$(Ala)_3$−NHMe, Tobias and Brooks;[12] blocked Ala_{13}, Daggett and Levitt.[13] Comparison to these studies, which used varying force fields and methods, shows that the highly populated regions are similar, the major difference with our study being the region of transition between the α_R and β regions. The majority of the transitions between these two states are over the barrier that corresponds to the higher energy barrier in our study. All of the studies used in the comparison either use blocking groups on the ends of the peptide or set the partial charges of the end groups to zero.

Schafer *et al*.[6] found that the interaction of the end groups can significantly affect the torsional states of other residues. We therefore ran two continuum solvent simulations, the first using the all-hydrogen CHARMM24 parameter set and the second using the CHARMM19 extended atom parameter set on the blocked alanine tetrapeptide (Ac−$(Ala)_4$−NHMe) with $\epsilon = 80$ (results not shown). We found the probability distributions along ϕ and ψ of both continuum solvent simulations to be very similar to our original simulations, but the distribution from the CHARMM19 extended atom simulation had the majority of the transitions between the α_R and β regions occurring over the barrier corresponding to the barrier of higher energy in our explicit solvent simulations. Therefore the force field and the presence of methyl blocking groups appear to be responsible for the small differences we observe between the distributions from our simulations and those of other alanine peptide simulations.

Conclusions

Although we were not able to completely sample all of the allowed conformational space for the alanine tetrapeptide in solution, we did obtain a complete sampling of the subset for all ϕ torsions near g^-, from which we can define four main states sampled by each of the simulations. The different end group charge combinations changed the populations of the four states (Figure 10). State 1 was preferred by (+/0) and (+/−) simulations, while state 2 was preferred by (0/−) and state 3 by (0/0). State 4 was almost equally populated by all four simulations. As previously mentioned, we did not observe any significant or stable classically defined reverse turn conformations in our simulations. PMF and kinetic analysis of the ψ dihedral transitions indicate that the end group charge has a local effect on the nearest dihedral on each end of the peptide. The charge state of the N-terminus strongly affects the distribution of ψ_1. The (+/0) and (+/−) simulations have one region populated for this dihedral, while the (0/0) and (0/−) simulations had two populated regions. The charge state of the C-terminus significantly affects the distributions of ϕ_4 and ψ_3. The distribution of ϕ_4 is shifted and is wider for the (0/−) and (+/−) simulations compared to the distribution of the same dihedral for the (0/0) and (+/0) simulations. The distribution of ψ_3 has two populated regions for all of the simulations, while the distribution between the two regions is affected the greatest amount by the charge state of the C-terminus. The local effects of the two terminal groups change the energetics and dynamics of the tetrapeptide in solution and account for the majority of the differences between the populations observed in our simulations.

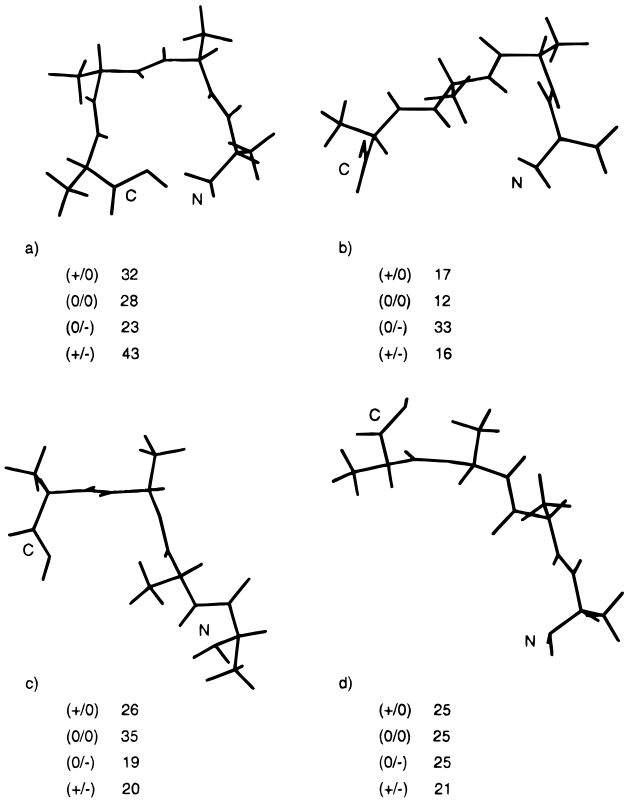

Figure 10. Stick plot of the four defined states with their population from each simulation: (a) state 1, (b) state 2, (c) state 3, (d) state 4.

Changing the charge state of the end groups modifies the electrostatic interactions of the peptide, which affects the stabilities of the peptide's conformations (*i.e.* relative populations). Wang *et al*.[14] compared the free energy change for the coil−helix equilibrium for blocked alanine chains of 1−14 residues long. The authors investigated the electrostatic contribution to helix stability by comparison of MD simulations in explicit water of the peptide with partial charges (full charge model) and with partial charges set to zero (zero charge model). They concluded that electrostatic interactions, including hydrogen bonds, slightly destabilize the helix, which results in a shift of the relative populations. In comparison, we observed a shift in the relative populations of the alanine tetrapeptide with each type of terminal group charge state.

The long-range interaction between the end groups of the tetrapeptide apparently has a minor but direct effect on the conformations, although coupling through solubility may be

more subtle. Perkyns *et al.*[29] studied conformationally dependent solubilities of the Gly−Ala−Gly zwitterion. Solubility is strongly dependent on molecular conformation and is a consequence of the size of the molecular dipole. The authors found that there are two dipole dependent contributions to the net relative free energy of solvation that are approximately equal and opposite in size, a solvent contribution that is inversely proportional to the dipole size, and a solute contribution that is proportional to the size of the molecular dipole. Comparing the (0/−) and (+/−) simulations, changing the N-terminus from uncharged to charged, shifts the preferred populated region from t to g^- in ψ_3. The change in the population is due to the formation of a transient salt bridge between the two charged end groups. Zimmerman and Scheraga[30] conclude from their study of blocked dipeptides in vacuo and of protein X-ray data that bends are stabilized primarily by local (intraresidue) forces compared to long-range interactions. Tobias *et al.*[11] found from their results on the conformational equilibria of the blocked alanine dipeptide that the extended conformations are favored in solution in the absence of stabilizing interresidue interactions involving side chains and/or charged terminal groups. If we consider states 1 and 2 in our simulations as an ensemble of folds or turns and states 3 and 4 as an ensemble of extended structures, then from the relative populations (Figure 10) for the neutral simulation (0/0) 40% of the structures are turns and 60% are extended; a slight preference for the extended ensemble. In the zwitterion simulation (+/−) 59% of the structures are turns and 41% are extended. The interaction between the charged end groups slightly stabilizes the turn ensemble and destabilizes the extended structure ensemble.

We expect that more complete sampling along the ϕ dihedrals will not qualitatively change the local effects observed in this study and would only influence the population(s) of the additionally sampled low-population state(s). It is well understood that most small peptides in solution exist in an equilibrium between conformational states. The results from our study show that this equilibrium is shifted by a change in the charge states of the terminal groups; this could have possible implications on experimental structural determination techniques such as using NOEs to determine time-averaged conformational state(s). Furthermore, results from our zwitterion simulation indicate that such events as ion pair formation are on a nanosecond time scale. This could affect the results of computational techniques such as free energy perturbation simulations which typically employ short windows (10−50 ps).

Acknowledgment. The authors would like to thank the Robert A. Welch Foundation and the National Institutes of Health for partial support. H.D.B. was supported by a fellowship from the Keck Center for computational Biology and Grant No. BIR-92-56580 from the National Science Foundation. This project was partially supported by the Kansas Agricultural Experimental Station (Publication 98-66-J). The Meta center is thanked for compulational support.

References and Notes

(1) Hruby, V. J.; Pettitt, B. M. In *Computer-Aided Drug Design: Methods and Applications*; Perun, T. J., Propst, C. L., Eds.; Marcel Dekker: New York, 1989; pp 405−460.
(2) Flippen-Anderson, J. L.; Hruby, V. J.; Collins, N.; George, C.; Cudney, B. *J. Am. Chem. Soc.* **1994**, *116*, 7523−7531.
(3) Holtzer, A.; Hawkins, R. B. *J. Am. Chem. Soc.* **1996**, *118*, 4220−4221.
(4) Bradley, E. K.; Thomason, J. F.; Cohen, F. E.; Kosen, P. A.; Kuntz, I. D. *J. Mol. Biol.* **1990**, *215*, 607−622.
(5) Dyson, H. J.; Rance, M.; Houghten, R. A.; Lerner, R. A.; Wright, P. E. *J. Mol. Biol.* **1988**, *201*, 161−200.
(6) Schafer, L.; Newton, S. Q.; Cao, M.; Peeters, A.; Van Alsenoy, C.; Wolinski, K.; Momany, F. A. *J. Am. Chem. Soc.* **1993**, *115*, 272−280.
(7) Young, W. S.; Brooks, C. L., III *J. Mol. Biol.* **1996**, *259*, 560−572.
(8) Tobias, D. J.; Brooks, C. L., III *J. Phys. Chem.* **1992**, *96*, 3864−3870.
(9) Anderson, A. G.; Hermans, J. *Proteins* **1988**, *3*, 262−265.
(10) Marrone, T. J.; Gilson, M. K.; McCammon, J. A. *J. Phys. Chem.* **1996**, *100*, 1439−1441.
(11) Tobias, D. J.; Sneddon, S. F.; Brooks, C. L., III *J. Mol. Biol.* **1990**, *216*, 783−796.
(12) Tobias, D. J.; Brooks, C. L., III *Biochem.* **1991**, *30*, 6059−6070.
(13) Daggett, V.; Levitt, M. *J. Mol. Biol.* **1992**, *223*, 1121−1138.
(14) Wang, L.; O'Connell, T.; Tropsha, A.; Hermans, J. *Biopolymers* **1996**, *39*, 479−489.
(15) Jorgensen, W. L.; Chandrasekhar, J.; Madura, J. D.; Imprey, R. W.; Klein, M. L. *J. Chem. Phys.* **1983**, *79*, 926−935.
(16) MacKerell, A. D., Jr.; Bashford, D.; Bellott, M.; Dunbrack, R. L., Jr.; Field, M. J.; Fischer, S.; Gao, J.; Guo, H.; Ha, S.; Joseph, D.; Kuchnir, L.; Kuczera, K.; Lau, F. T. K.; Mattos, C.; Michnick, S.; Ngo, T.; Nguyen, D. T.; Prodhom, B.; Roux, B.; Schlenkrich, M.; Smith, J. C.; Stote, R.; Straub, J.; Wiorkiewicz-Kuczera, J.; Karplus, M. *FASEB J.* **1992**, *6*, A143.
(17) Ewald, P. *Ann. Phys.* **1921**, *64*, 253−287.
(18) Smith, P. E.; Pettitt, B. M. *Comput. Phys. Commun.* **1995**, *91*, 339−344.
(19) York, D. M.; Darden, T. A.; Pedersen, L. G. *J. Chem. Phys.* **1993**, *99*, 8345−8348.
(20) Ryckaert, J. P.; Ciccotti, G.; Berendsen, H. J. C. *J. Comput. Phys.* **1977**, *23*, 327−341.
(21) Zhang, Y.; Pastor, R. W. *Mol. Simul.* **1994**, *13*, 25−38.
(22) Eisenberg, D.; Kauzmann, W. *The Structure and Properties of Water*; Oxford University Press: Oxford, 1969.
(23) Cooke, R.; Kuntz, I. D. *Annu. Rev. Biophys. Bioeng.* **1974**, *3*, 95−126.
(24) Tasaki, K.; McDonald, S.; Brady, J. W. *J. Comput. Chem.* **1993**, *14*, 278−284.
(25) Smith, P. E.; Pettitt, B. M. *J. Phys. Chem.* **1994**, *98*, 9700−9711.
(26) Smith, P. E.; Dang, L. X.; Pettitt, B. M. *J. Am. Chem. Soc.* **1991**, *113*, 67−73.
(27) Smith, P. E.; Pettitt, B. M.; Karplus, M. *J. Phys. Chem.* **1993**, *97*, 6907−6913.
(28) Smith, P. E.; Blatt, H. D.; Pettitt, B. M. *Proteins: Struct., Funct. Genet.*, in press.
(29) Perkyns, J. S.; Wang, Y.; Pettitt, B. M. *J. Am. Chem. Soc.* **1996**, *118*, 1164−1172.
(30) Zimmerman, S. S.; Scheraga, H. A. *Proc. Natl. Acad. Sci. U.S.A.* **1977**, *74*, 4126−4129.